Published OnlineFirst February 1, 2012; DOI:10.1158/1541-7786.MCR-11-0508

Molecular Cancer Research

MYC-Driven Tumorigenesis Is Inhibited by WRN Syndrome Gene Deficiency

Russell Moser, Masafumi Toyoshima, Kristin Robinson, et al.

Mol Cancer Res 2012;10:535-545. Published OnlineFirst February 1, 2012.

Published OnlineFirst February 1, 2012; DOI:10.1158/1541-7786.MCR-11-0508

DNA Damage and Cellular Stress Responses

Molecular Cancer Research

MYC-Driven Tumorigenesis Is Inhibited by WRN Syndrome Gene Deficiency

Russell Moser[1], Masafumi Toyoshima[1], Kristin Robinson[1], Kay E. Gurley[1], Heather L. Howie[1], Jerry Davison[2], Martin Morgan[2], Christopher J. Kemp[1], and Carla Grandori[1,3]

Abstract

MYC-induced DNA damage is exacerbated in WRN-deficient cells, leading to replication stress and accelerated cellular senescence. To determine whether WRN deficiency impairs MYC-driven tumor development, we used both xenograft and autochthonous tumor models. Conditional silencing of WRN expression in c-MYC overexpressing non–small cell lung cancer xenografts impaired both tumor establishment and tumor growth. This inhibitory effect of WRN knockdown was accompanied by increased DNA damage, decreased proliferation, and tumor necrosis. In the Eμ-Myc mouse model of B-cell lymphoma, a germline mutation in the helicase domain of Wrn ($Wrn^{\Delta hel/\Delta hel}$) resulted in a significant delay in emergence of lethal lymphomas, extending tumor-free survival by more than 30%. Analysis of preneoplastic B cells from Eμ-Myc Wrn mutant mice revealed increased DNA damage, elevation of senescence markers, and decreased proliferation in comparison with cells from age-matched Eμ-Myc mice. Immunohistochemical and global gene expression analysis of overt Eμ-Myc $Wrn^{\Delta hel/\Delta hel}$ lymphomas showed a marked increase in expression of the CDK inhibitor, $p16^{Ink4a}$, as well as elevation of TAp63, a known mediator of senescence. Collectively, these studies show that in the context of Myc-associated tumorigenesis, loss of Wrn amplifies the DNA damage response, both in preneoplastic and neoplastic tissue, engaging activation of tumor suppressor pathways. This leads to inhibition of tumor growth and prolonged tumor-free survival. Targeting WRN or its enzymatic function could prove to be an effective strategy in the treatment of MYC-associated cancers. *Mol Cancer Res; 10(4); 535–45. ©2012 AACR.*

Introduction

We previously showed that *WRN*, a gene encoding a RecQ DNA helicase, is a direct transcriptional target of c-MYC, and that the absence of WRN causes MYC overexpressing, *h-Tert* immortalized cells to undergo senescence (1). Mechanistically, the MYC/WRN codependence has been explained by the recent demonstration that MYC directly influences the DNA prereplication machinery, and that MYC overexpression dramatically accelerates S-phase, thereby sensitizing cells to "replication stress" (2). Inhibition of WRN function in MYC overexpressing cells leads to excessive accumulation of DNA damage at sites of newly replicated DNA, triggering activation of the ATR–CHK1 pathway and, in turn, forcing the cells into a nonproliferative, senescent state (3). Thus, MYC transcriptional stimulation of the *WRN* gene provides a feed-forward mechanism to limit MYC-associated DNA replication stress and enables continued cell proliferation.

Mutations in the *WRN* gene are associated with a progeroid syndrome in humans [Werner syndrome (WS)], which is characterized by accelerated aging, cellular senescence, genomic instability, and an increased incidence of otherwise rare cancers of mesenchymal origin (4, 5). *WRN* encodes a multifunctional protein with both DNA helicase and exonuclease activity, a property which sets WRN as the exception among other members of the RecQ family, which harbor only a DNA helicase domain (6, 7). WRN protein binds to and modifies DNA secondary structures that are likely to arise during DNA replication (8, 9). This property of WRN protein is consistent with its role in repair/recovery from replication-associated damage (10, 11). The role of WRN in maintaining DNA fidelity, coupled with the tumor predisposition of WS patients, has suggested that *WRN* could function as a tumor suppressor gene. However, *WRN* mutations have not been reported in tumors, and we and others have found that WRN and other members of the RecQ helicase family are significantly overexpressed in cancer cell lines derived from Burkitt's lymphoma, neuroblastoma, breast, ovarian, and lung cancers (C. Grandori;

Authors' Affiliations: Divisions of [1]Human Biology and [2]Public Health Science, Fred Hutchinson Cancer Research Center; and [3]Quellos High Throughput Screening Core, Department of Pharmacology, University of Washington School of Medicine, Seattle, Washington

Note: Supplementary data for this article are available at Molecular Cancer Research Online (http://mcr.aacrjournals.org/).

R. Moser and M. Toyoshima contributed equally to this work.

Corresponding Authors: Carla Grandori, Division of Human Biology, Fred Hutchinson Cancer Research Center, Seattle, WA 98109. Phone: 206-667-1835; Fax: 206-667-5815; E-mail: cgrandor@fhcrc.org; and Christopher J. Kemp. Phone: 206-667-4252; Fax: 206-667-5815; E-mail: cjkemp@fhcrc.org

doi: 10.1158/1541-7786.MCR-11-0508

Published OnlineFirst February 1, 2012; DOI:10.1158/1541-7786.MCR-11-0508

unpublished results and ref. 12). Furthermore, whereas fibroblasts from Wrn mutant mice exhibit enhanced sensitivity to DNA cross-linking agents, characteristic of human WS cells (13, 14), Wrn-deficient mice have not shown a predisposition to spontaneous tumor development. These observations, together with the prosurvival role of WRN in MYC overexpressing cells, suggest WRN could play a supporting role in the context of MYC-dependent tumorigenesis and consequently, its deficiency might inhibit rather than accelerate tumor development. Here, we establish that acute WRN depletion in MYC overexpressing human lung cancer xenografts blocks tumor growth and further, that germline Wrn deficiency in mice causes a significant delay in Myc-induced lymphomagenesis and prolongs tumor-free survival. Thus, in the context of Myc-driven cancers, Wrn provides a critical prosurvival function that is necessary for efficient tumor growth and constitutes a candidate druggable target in tumors driven by an "undruggable" oncogenic driver.

Materials and Methods

Mouse strains, genotyping, and tumor monitoring

The $Wrn^{\Delta hel/\Delta hel}$ mutation (14) was backcrossed onto C57BL/6 mice to purity (N20). The C57BL/6 *Eμ-Myc* transgenic mouse strain (15) was interbred to C57BL/6 $Wrn^{\Delta hel/\Delta hel}$ mice to generate *Eμ-Myc* $Wrn^{\Delta hel/+}$ and $Wrn^{\Delta hel/+}$ mice, which were subsequently intercrossed and backcrossed to parental lines to generate nontransgenic and *Eμ-Myc* transgenic $Wrn^{+/+}$ and $Wrn^{\Delta hel/\Delta hel}$ experimental animals (F_1 generation). Mice were monitored daily for signs of morbidity and tumor development. Moribund animals were sacrificed and tumors and lymphoid organs were harvested for histopathologic and molecular analysis. Germline transmission of the *Eμ-Myc* transgene, and the Werner helicase domain deletion (*Wrn* Δdel exon 3–4) was confirmed using conventional PCR–based genotyping strategies (14, 15). All animal protocols were approved by the Fred Hutchinson Cancer Research Center Laboratory Animal Care and Use Committee.

Immunoblotting of lymphomas

Whole cell protein extracts from primary pre-B cells and B-cell tumors from *Eμ-Myc* and *Eμ-Myc* $Wrn^{\Delta hel/\Delta hel}$ transgenic mice were isolated as previously described (16). Equal amounts of clarified lysates (100–150μg per lane) were analyzed by Western blotting with antibodies specific to mouse p19Arf (5-C3-1), p16Ink4a (M-156), Mdm2 (C-18) pAb, and Actin (I-19) from Santa Cruz Biotechnology, Mdm2 (MD-219-Abcam) mAb, Cyclin D1 (DCS6), pH2A.X (ser139), pAtr (ser424) p53 (ser18), and cleaved caspase-3 (Asp175) from Cell Signaling Technology, and p53 (CM5) from Novocastra. Detection was by enhanced chemiluminescence (Supersignal–Thermo Scientific).

Acidic β-galactosidase assay

The senescence-associated β-galactosidase assay (SA-β-gal) was carried out as previously described with some modifications (17, 18). Briefly, murine tissues were harvested and frozen gradually (CO_2) in cryomolds within OCT compound and stored at −80°C. Cryosections of tissues were cut using a cryotome at 6 to 12 μm, fixed in 0.5% glutaraldehyde (6-μm section/15 minutes) at room temperature (22°C), and rinsed with PBS (pH 7.3). Tissue sections were then covered with fresh SA-β-gal stain [40 mmol/L citric acid/sodium phosphate (pH 6.0), 1 mg/mL Xgal (DMF), 5 mmol/L potassium ferricyanide, 5 mmol/L ferrocyanide, 150 mmol/L NaCl, 2 mmol/L $MgCl_2$] placed in humidity chambers, and incubated at 37°C in an ambient 21% O_2 environment for 6 to 8 hours. After staining, tissue sections were rinsed with PBS and processed via standard immunohistochemical protocols.

Flow cytometric analysis of B-cell proliferation and apoptosis

Single-cell suspensions of bone marrow cells and splenocytes were prepared by harvesting marrow from femurs, disassociating the spleens between frosted microscope slides and filtering both cell preparations through nylon cell strainers. For analysis of differentiation status, splenic cells were incubated with PE-conjugated anti-CD45R/B220 and PerCP-Cy5.5–conjugated anti-IgM antibodies (BD Biosciences Pharmingen). Proliferation rates were measured using a fluorescein isothiocyanate (FITC) 5-bromo-2′-deoxyuridine (BrdUrd) Flow Kit (BD Biosciences Pharmingen) as described by the manufacturer. Animals were injected with BrdUrd (40 mg/gram body weight, intraperitoneally), and bone marrow and spleen were harvested 2 hours later. Apoptosis in pre-B ($B220^+/IgM^-$) and B-cell ($B220^+/IgM^+$) populations from spleen and bone marrow was measured using FITC-conjugated antiactive caspase-3 (BD Biosciences Pharmingen). All samples were analyzed by a FACSCalibur (Becton-Dickinson).

Splenocyte isolation and immunoblotting

Single-cell suspensions were generated from spleens of *Eμ-Myc* and *Eμ-Myc* $Wrn^{\Delta hel/\Delta hel}$ mice as previously described (19). Cell suspensions were suspended in a hypotonic buffer to lyse red blood cells, and splenic lymphocytes and cellular debris were separated via centrifugation along a ficoll-hypaque (d = 1.077) gradient (800 × *g* at 4°C for 15 minutes). Isolated splenocytes were then lysed in 50 mmol/L Tris (pH 8.0), 200 mmol/L NaCl, 5 mmol/L EDTA, 1% Triton X-100, 10% Glycerol, 1 mmol/L $NaVO_4$, 2 mmol/L DTT, 1.5 μg/mL aprotinin, 0.3 mg/mL pefabloc, 6 μg/mL leupeptin. Equal amounts of clarified protein lysates (50 μg per lane) were analyzed by Western blotting with antibodies to phospho-H2A.X (Serine 139), phospho-Atr (Serine 428), phospho-p53 (Serine18) from Cell Signaling Technology, p53 (CM5) from Novocastra, and β-Actin from BioVision.

Sequence analysis of lymphomas

Total RNA was isolated from select lymphomas using TRIzol (Invitrogen) followed by Qiagen RNeasy Mini Kit (Qiagen). The first strand cDNA was synthesized with dT oligos from Superscript III first strand kit (Invitrogen). p53

Published OnlineFirst February 1, 2012; DOI:10.1158/1541-7786.MCR-11-0508

cDNA was amplified using the primer set for exons 2–11 (p53-fwd: 5′-GCTTCTCCGAAGACTGGATGACT-3′ and p53-rev: 5′-GATTGTGTCTCAGCCCTG AAGTCA-3′; ref. 20). A second primer set for exons 5–8 (p53-fwd-Ex5: 5′-GTACC TTATGAGCCACCCGA-3′ and p53-rev-Ex8: 5′-TTTTCTTTTGCGGGGGA-3′) was used for confirmation of sequence fidelity. PCR products were sequenced via ABI 3730xl DNA Analyser (Applied Biosystems) using the same primer sets. Sequencing data were aligned to *Mus musculus p53* mRNA transcript sequences [ENSMUSP00000104298, . . .104297, . . .005371; www.ensembl.org]. Biallelic deletions of the *Cdkn2a (Ink4a/ARF)* locus were also examined from select lymphomas via PCR of genomic exons 1α, exon1β, exon 2, and exon 3.

Immunohistochemical staining of lymphomas

Tissues were fixed in normal buffered formalin (NBF), processed to paraffin and stained for hematoxylin and eosin (H&E), specific proteins, BrdUrd, or terminal deoxynucleotidyl transferase dUTP end labeling (TUNEL). Staining for p53 (Vector), p19Arf (Santa Cruz), Histone H3 (Serine10; Cell Signaling Technology), Histone H2A.X (Serine139; Cell Signaling Technology), and cleaved caspase-3 (Cell Signaling Technology) were done using a standard 3-step ABC method. Slides were developed using DAB/NiCl (Sigma) and counterstained with methyl green. Sections for BrdUrd (Dako) staining were treated with HCl and trypsin before incubating with primary antibody. For TUNEL staining, Trevigen TACS2 TdT kit was used as per manufacturer's instructions.

Expression analysis and *in vitro* assay of Wrn-mediated knockdown

RNA was extracted from mouse tissue using the RNAeasy Kit (Qiagen), reverse transcribed using a Superscript II RT Kit (Invitrogen). The following probe sets were used for quantitative reverse transcriptase PCR (qRT-PCR) analysis: Wrn helicase domain (Mm00499253_m1), Wrn C-terminus (Mm01197916_m1), Bcl-2 (Mm004380-70_m1), Prkdc (Mm01342967_m1), and Trp63 (Mm00495788_m1; Applied Biosystems–Life Technologies Inc.). cDNAs were subjected to qRT-PCR analysis using a SYBR green PCR Master Mix (Applied Biosystems) with primers specific to TAp63 (forward, 5′-TGCCCCGACCCTTACATCCA-3′; reverse, 5′-GGAAGGACACATCGAAGCTGTG-3′); dNp63 (forward, 5′-CTGGAAAACAATGCCCAGAC-3′; reverse, 5′-GAGGAGCCGTTCTGAATCTG-3′); β-actin (forward, 5′-GATCTGGCACCACACCTTCT-3, reverse, 5′-GGGGTGTTGAAGGTCTCAAA-3′; refs. 21, 22). For *in vitro* assays, single-cell suspensions were isolated from *Eμ-Myc* lymphomas as above and grown in B-cell media [Dulbecco's modified Eagle's medium (DMEM)/IMEM supplemented with 10% FBS and β-mercaptoethanol] on an NIH3T3 fibroblast feeder layer. Retroviral vectors were constructed using pLMP (gifted from Dr. Paddison) and siRNAs (Ambion) targeting the following sequences: shWRN1(CTGTGTGTGTCTGAGAGCAAAT; shWRN2(AACCCAGAACTTGACAGTTTAG, shControl (CAACAAGATGAAGAGCACCAA). Retroviral infections were done using a phoenix ecotropic packaging cell line with helper plasmid pPEM5 (gifted from Dr. Miller). B-cell lymphoma cells were infected via "spinoculation," 1500 RPM for 10 minutes at 32°C, through 4 successive inoculations with retroviral containing supernatant from the phoenix cells supplemented with polybrene (Schmitt C; personal communication). B-cell lymphoma cells were again cultured on an NIH3T3 feeder layer and selected with puromycin for 3 days and harvested for gene expression at 6 to 8 days postinfection.

Microarray hybridization and data analysis

Total RNA was isolated from 4 lymphomas from each genotype using TRIzol (Invitrogen) and RNeasy Kit (Qiagen), labeled using the Message AMP Kit (Ambion) and hybridized to Illumina BeadStudio Gene Expression microarray MouseRef 8v2 (Illumina Inc.). Expression data were processed using the Illumina GenomeStudio software, using quantile normalization and background subtraction. Nonspecific probe filtering of the array data was done using a GenomeStudio-reported detection *P* value cutoff of 0.1, reducing the number of genes to a filtered dataset of 7,865. The R/Bioconductor arrayQualityMetrics package was used to assess the quality of the BeadArray data as adequate for analysis. We used the R/Bioconductor stats package heatmap function to calculate hierarchical clustering dendrograms. In addition, the Bioconductor package lumi was used for affy-like background subtraction and to quantile normalize the full dataset. Negative control features were used to estimate signal-to-noise ratios across the entire dataset. For a given gene, if s/n < 3 across all arrays, the gene was removed from further analysis. The Bioconductor package limma was used to carry out modified *t* statistic significance testing (23) and multiple testing corrections using Benjamini and Hochberg (24). All microarray data (MIAME compliant) are deposited in NCBI's Gene Expression Omnibus (25) and are accessible through GEO Series accession number (GSE25671).

Lentiviral shRNA construction and packaging

Lentiviral constructs for each short hairpin RNA (shRNA) and a scramble were designed and constructed in a pLenti6-tts system using the Gateway LR Clonase. Stbl3 chemically competent cells (Invitrogen) were transformed with 1 to 5 ng of DNA, and clones were selected on blasticidin (50 μg/mL) LB isolated, screened, and propagated. 293FT cell line (derived from 293F cells, stably expressing the SV40 large T antigen for enhanced virus production) was cultured in DMEM/10%FBS/500 μg/mL G418/pen/strep ViraPower Packaging Mix (Invitrogen) and resuspended in 195 μL of sterile water to a concentration of 1 μg/μL. When cotransfected with the pLenti-DEST expression construct into the 293FT producer cell line, this mixture of plasmids supplies the viral proteins in *trans* that are required to create viral products. Viral supernatants were generated using 293FT cells transfected with 10 μg shRNA plasmid using Lipofectamine 2000 and the appropriate lentiviral packaging plasmid DNA (ViraPower). The media was changed 16 hours

Published OnlineFirst February 1, 2012; DOI:10.1158/1541-7786.MCR-11-0508

after transfection and the virus was harvested 48 to 56 hours later. Viral supernatant was filtered (0.40 μm), aliquoted and frozen at −80 for subsequent use.

Lentiviral mediated knockdown of WRN protein in A549 lung carcinoma cells

Human A549 small cell lung carcinoma cells (American Type Culture Collection) cultured in DMEM/10%FBS/pen/strep were infected with lentiviral tet-mediated vectors with shRNA scramble control (19-mer–GUUGUUCUACUUCUCGUGG), shWRN-I (19-mer seq–GUCUAUCCGCUGUAGCAAU), shWRN-II (19-mer seq–GUACCUUAUCCACAUGGCA), or shWRN-III (19 mer seq–GAGACAAAUCAUCUUGUCU) 5′–3′ target sequences and knockdown of the WRN protein was assessed via immunoblot 48 hours posttreatment with 0.01 μg/mL doxycycline (Sigma D9891) in culture media. Immunoblots were probed with WRN pAb (H-300), Actin (I-19), and c-Myc (N-262) antibodies purchased from Santa Cruz Biotechnology.

Xenograft tumor models

A549 cells were freshly infected with either the lentiviral tet-mediated shRNA scramble control or the shWRN-I (Fig. 1E and F) or shWRN II (Fig. 1G and H) and 2.5×10^6 cells in 0.2 mL PBS were inoculated subcutaneously into the left and right flanks of 10 eight-week-old nonobese diabetic–severe combined immunodeficient (NOD-SCID) gamma null mice, respectively. For the experiment of Fig. 1E and F (shWRN I), FOXN1 (nu/nu) nude mice were exposed to doxycycline from day 1. For the experiment of Fig. 1G and H (shWRN II), NOD-SCID gamma null mice were given doxycycline (2 mg/mL in 5% sucrose) *ad libitum* in their drinking water ($n = 5$), only when tumors had reached a visible size, whereas an equal number of mice received only 5% sucrose water. The volume of the implanted tumor was measured every 2 to 3 days with a caliper, using the formula: $V = L \times W^2/2$; in which V, volume (mm^3); L, biggest diameter (mm); W, smallest diameter (mm). A tumor was defined as a palpable mass of 100 mm^3 or more volume. Mice were sacrificed at 3 to 4 weeks.

Statistical analysis

All images shown are representative of at least 10 fields viewed over 2 stained sections per animal. Quantitation was done using 10 fields per animal. All columns represent mean ± SEM, unless otherwise noted. All statistical analyses were done using unpaired 2-tailed t test unless otherwise indicated. Statistical analysis of Kaplan–Meier survival curves was done via log-rank (Mantel–Haenszel) test (Graphpad Software) or SPSS (IBM, Worldwide).

Results

WRN is critical for establishment and growth of non–small cell lung cancer cells with MYC overexpression

To examine the role of WRN in a model of Myc-associated cancer, the growth rates of A549 non–small cell lung carcinoma (NSCLC) xenografts were monitored after WRN knockdown. A549 cells express high levels of c-MYC, as confirmed via Western blot analysis (Fig. 1A). Three shRNAs against WRN were first tested in transient assays in 293T cells. shWRN I and shWRN II indicated the best knockdown (data not shown). A549 cells were transduced with lentiviral vectors expressing doxycycline-conditional shWRN I or shWRN II specific to the *WRN* gene. Knockdown was measured by Western blot analysis (Fig. 1B) and through a time course of WRN mRNA following shWRN I (Fig. 1D). The latter indicated that optimal knockdown occurred several days after shRNA induction, consistent with the long half-life of WRN protein and mRNA. To determine the effect of WRN depletion on the growth of A549 cancer cells, long-term colony assays were carried out. In A549 cells harboring a control shRNA, growth was not affected by doxycycline treatment, whereas cells expressing the WRN-specific shRNA showed a dramatic inhibition of growth following addition of doxycycline (Fig. 1C). We next wished to test the role of WRN in tumor establishment and growth in 2 xenograft models. One, in which expression of the shRNA was initiated at the time of tumor cell injection, and a second, a therapeutic model in which tumors were established before WRN knockdown. Figure 1F shows the tumor size over time in 4 mice, in which each mouse was injected on one flank with A549 cells transduced with a control shRNA and on the other with shWRN I. Mice were exposed to doxycycline from the day of implantation to induce shRNA expression. A representative mouse showing inhibition of tumor growth by WRN knockdown is shown in Fig. 1E. The results obtained with the therapeutic model are shown in Fig. 1G and H, in which 10 mice (5 in each arm sh control and shWRN II) were exposed to doxycyline after tumors reached approximately 100 mm^3. In this therapeutic model, A549 tumor growth was markedly inhibited by shWRN II induction. Representative xenografts are shown in Fig. 1G. Thus WRN depletion with 2 different hairpins in 2 settings markedly inhibited tumor establishment and growth. WRN-depleted xenografts displayed a prominent increase in DNA damage, an increase in necrosis, and a reduction in proliferative cells (Fig. 2A and B). However, no significant difference in caspase-3–dependent apoptosis compared with controls was observed (Fig. 2C). Together, these results established that impaired tumor growth caused by WRN depletion is due to increased DNA damage and reduced proliferation.

Wrn deficiency delays Eμ-Myc–induced lymphomagenesis and prolongs tumor-free survival

As the immune system and tumor microenvironment profoundly affect tumor development, we next addressed the role of Wrn in an autochthonous model of tumorigenesis in immunocompetent mice. To this end, we assessed the impact of a germline Wrn helicase mutation ($Wrn^{\Delta hel/\Delta hel}$; ref. 14) on tumor latency in the Eμ-Myc mouse model. *Eμ-Myc* mice constitutively express c-myc in lymphoid precursor cells, leading to pre-B cell hyperplasia and subsequent lymphoma development (15). Cohorts of *Eμ-Myc* ($n = 41$),

Published OnlineFirst February 1, 2012; DOI:10.1158/1541-7786.MCR-11-0508

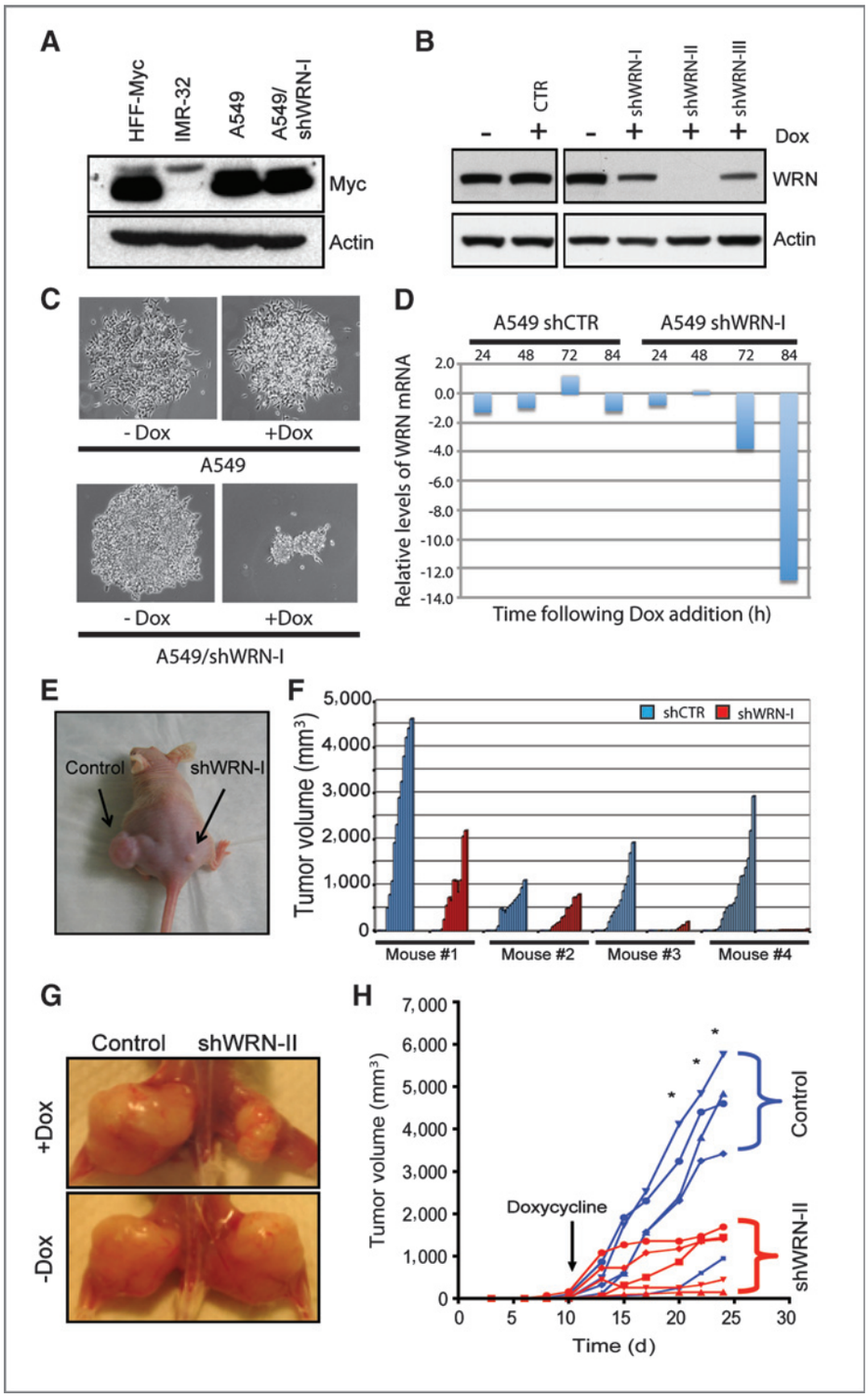

Figure 1. WRN knockdown suppresses tumor growth. A, Myc protein levels in A549 NSCLC cells with or without shWRN-I. HFF-Myc is shown as positive control for c-Myc expression, and IMR-32 cells are shown as a negative control for c-Myc expression. Actin was used as a loading control. B, WRN protein levels in A549 cells transduced with doxycycline (Dox)-conditional lentiviral vectors harboring WRN or control shRNAs (CTL) in the presence or absence of Dox. Actin was used as a loading control. C, long-term colony forming assay of A549 cells with control (top) or WRN-specific shRNAs (bottom) in the presence or absence of Dox. D, time course of WRN mRNA knockdown measured by qRT-PCR in A549 cells after addition of doxycycline to induce expression of shWRN I. E, representative image of an A549 xenograft at time of sacrifice showing a significant difference in tumor volume between negative control shRNA (left flank) and shWRN I (right flank). F, tumor volume of xenografts expressing shWRN I and sh control over a 2-week interval while mice were exposed to Dox since the time of implantation. G, representative image of the therapeutic xenograft model following induction of shWRN II or control shRNA with Dox in established A549 tumors. H, tumor volume of xenografts indicating the growth inhibition of shWRN II expressing tumors. Asterisk denotes a significant difference in mean tumor volume ($n = 5$) between control and shWRN II at indicated times postinjection, $P < 0.05$ (unpaired t test).

Eμ-Myc $Wrn^{\Delta hel/\Delta hel}$ ($n = 50$), as well as wild-type ($n = 30$) and $Wrn^{\Delta hel/\Delta hel}$ ($n = 30$) mice were followed for more than 2 years and Kaplan–Meier survival curves were generated. Virtually all *Eμ-Myc* mice developed lymphomas, but the median latency in *Eμ-Myc* $Wrn^{\Delta hel/\Delta hel}$ mice (151 days) was significantly delayed relative to *Eμ-Myc* mice (115 days; Fig. 3A). Control wild-type and $Wrn^{\Delta hel/\Delta hel}$ mice did not develop any related pathology over the same timespan (data not shown). To confirm the transcriptional induction of Wrn by c-Myc overexpression, previously

Published OnlineFirst February 1, 2012; DOI:10.1158/1541-7786.MCR-11-0508

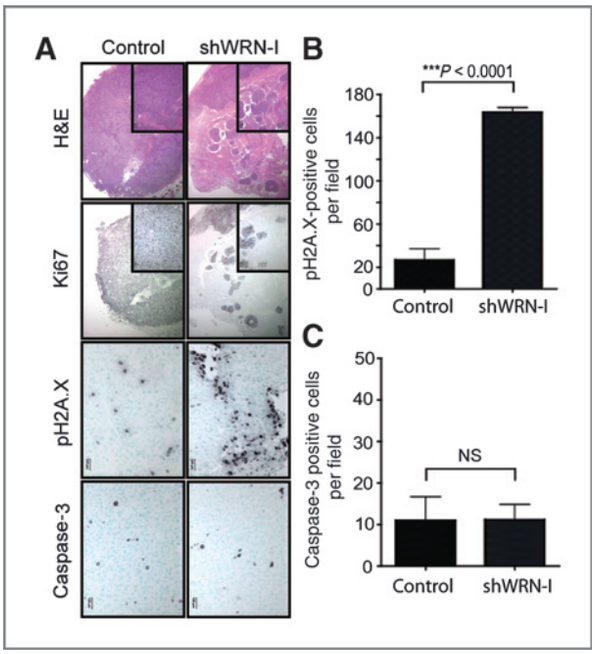

Figure 2. Immunohistochemical profiling of A549 NSCLC xenografts indicates increased DNA damage and decreased proliferation following WRN knockdown. A, representative IHC images from A549 xenografts showing decreased proliferation (H&E and Ki67) and increased DNA damage (γ-H2A.X, Serine139) in WRN-depleted xenografts (shWRN I) versus control xenografts (shCTL). In contrast no difference in apoptosis as judged by cleaved caspase-3 was detectable. H&E and Ki67 images show 10× field with 40× field inset. B, quantitative scoring of DNA damage (H2A.X Serine 139) from control and shWRN xenografts. Bars represent mean ± SD; $n = 3$ mice per graft, ten 40× fields per mouse, ***, $P < 0.0001$ (unpaired t test). C, quantitative scoring of apoptosis (cleaved caspase-3) from control and shWRN xenografts. Bars represent mean ± SD; $n = 3$ mice per graft, ten 40× fields per mouse, no significant difference via unpaired t test.

observed *in vitro* (1), Wrn protein and mRNA expression was measured in normal spleen and lymphomas from *Eμ-Myc* mice. Wrn protein levels were indeed elevated in both preneoplastic and lymphoma-derived cells from *Eμ-Myc* mice (Supplementary Fig. S1). In addition, expression of the truncated Wrn protein was verified in tissues from $Wrn^{\Delta hel/\Delta hel}$ mice (Supplementary Fig. S2). Together, these results highlighted a protumorigenic role for the Wrn DNA helicase in a well-documented model of Myc-driven tumorigenesis.

Wrn deficiency triggers a DNA damage response leading to proliferation arrest in the preneoplastic stage of tumor development

To address the basis for the impaired lymphomagenesis in *Eμ-Myc* $Wrn^{\Delta hel/\Delta hel}$ mice, we established another mouse cohort to examine markers of proliferation, apoptosis, and DNA damage in preneoplastic splenocytes before emergence of lymphomas. Preneoplastic B cells isolated from both bone marrow and spleen from *Eμ-Myc* $Wrn^{\Delta hel/\Delta hel}$ mice showed reduced proliferation compared with *Eμ-Myc* mice (Fig. 3B). Quantification of cleaved caspase-3–positive cells indicated that apoptosis was not significantly elevated in Wrn-deficient preneoplastic cells (Fig. 3C). Analysis of cell surface markers indicated that Wrn deficiency does not impinge on B cell homeostasis, as judged by the similar ratio of pre-B cell precursors versus mature B cells in *Eμ-Myc* mice from both *Wrn* genotypes (Fig. 3D). Consistent with reduced proliferation markers and the known role of Wrn in cellular senescence, a prominent increase in senescence-associated β-galactosidase (SA-β-gal) staining was observed in preneoplastic B-cell compartments (germinal center follicles of the spleen) from *Eμ-Myc* $Wrn^{\Delta hel/\Delta hel}$ mice compared with *Eμ-Myc* mice (Fig. 3E). Longitudinal immunoblot analysis indicated an increase in the accumulation of γ-H2AX (Serine 139), Atr (Serine 428), and p53 (Serine18) in preneoplastic splenocytes from *Eμ-Myc* $Wrn^{\Delta hel/\Delta hel}$ mice (Fig. 3F). Thus, Wrn deficiency blocks the expansion of preneoplastic cells by triggering a DNA damage response that impairs cell proliferation and favors senescence, thereby delaying the emergence of overt tumors.

Wrn deficiency delays lymphomagenesis by engaging tumor suppressor pathways

Previous research using the Eμ-Myc mouse model has shown that development of lymphomas coincides with either biallelic deletions in the *Cdkn2a* locus or mutation in the *p53* tumor suppressor (16, 26, 27). To further elucidate the mechanism by which Wrn deficiency delays lymphomagenesis, p53, $p19^{Arf}$, $p16^{Ink4a}$, cyclin D1, and cleaved caspase-3 were examined in *Eμ-Myc* and *Eμ-Myc* $Wrn^{\Delta hel/\Delta hel}$ lymphomas. We observed a striking elevation of the cyclin-dependent kinase (CDK) inhibitor $p16^{Ink4a}$ in the majority of *Eμ-Myc* $Wrn^{\Delta hel/\Delta hel}$ (82%) compared with *Eμ-Myc* (33%) lymphomas (Fig. 4A, Supplementary Fig. S3A, *, $P = 0.006$). $p16^{Ink4a}$ normally functions to sequester Cdk4, allowing for the degradation of cyclin D1 and release of $p27^{Kip1}$ from cyclin D1–Cdk4 complexes. Ultimately, this engages a G_1 cell-cycle arrest through Rb activation (28). Consistent with this role for $p16^{Ink4a}$, cyclin D1 levels were found to be reduced in *Eμ-Myc* $Wrn^{\Delta hel/\Delta hel}$ lymphomas, particularly late onset lymphomas with high $p16^{Ink4a}$ expression (Fig. 4A, asterisk indicates late onset). In addition, proliferation was significantly decreased in the *Eμ-Myc* $Wrn^{\Delta hel/\Delta hel}$ (Fig. 4B and C) lymphomas. Consistent with our data from preneoplastic tissue, no elevation of caspase-3–dependent apoptosis was observed in *Eμ-Myc* $Wrn^{\Delta hel/\Delta hel}$ lymphomas (Fig. 4A).

We next assessed the frequency of *p53* mutation in lymphomas. The results showed no significant difference in *p53* mutation between *Eμ-Myc* lymphomas (35%) and *Eμ-Myc* $Wrn^{\Delta hel/\Delta hel}$ lymphomas (45%; Supplementary Fig. S3A, $P = 0.748$). Furthermore, all tumors with stabilized p53 had mutations in *p53*, as previously reported (ref. 16; Supplementary Fig. S3B). The tumor suppressor $p19^{Arf}$ was overexpressed in lymphomas with high p53, consistent with its known role in p53 stabilization (ref. 29; Fig. 4A, Supplementary Fig. S3B). Proliferation and apoptosis were next assessed in late onset lymphomas, stratified for mutations in p53, anatomical location, and expression of $p16^{Ink4a}$ and $p19^{Arf}$. These results indicated

Published OnlineFirst February 1, 2012; DOI:10.1158/1541-7786.MCR-11-0508

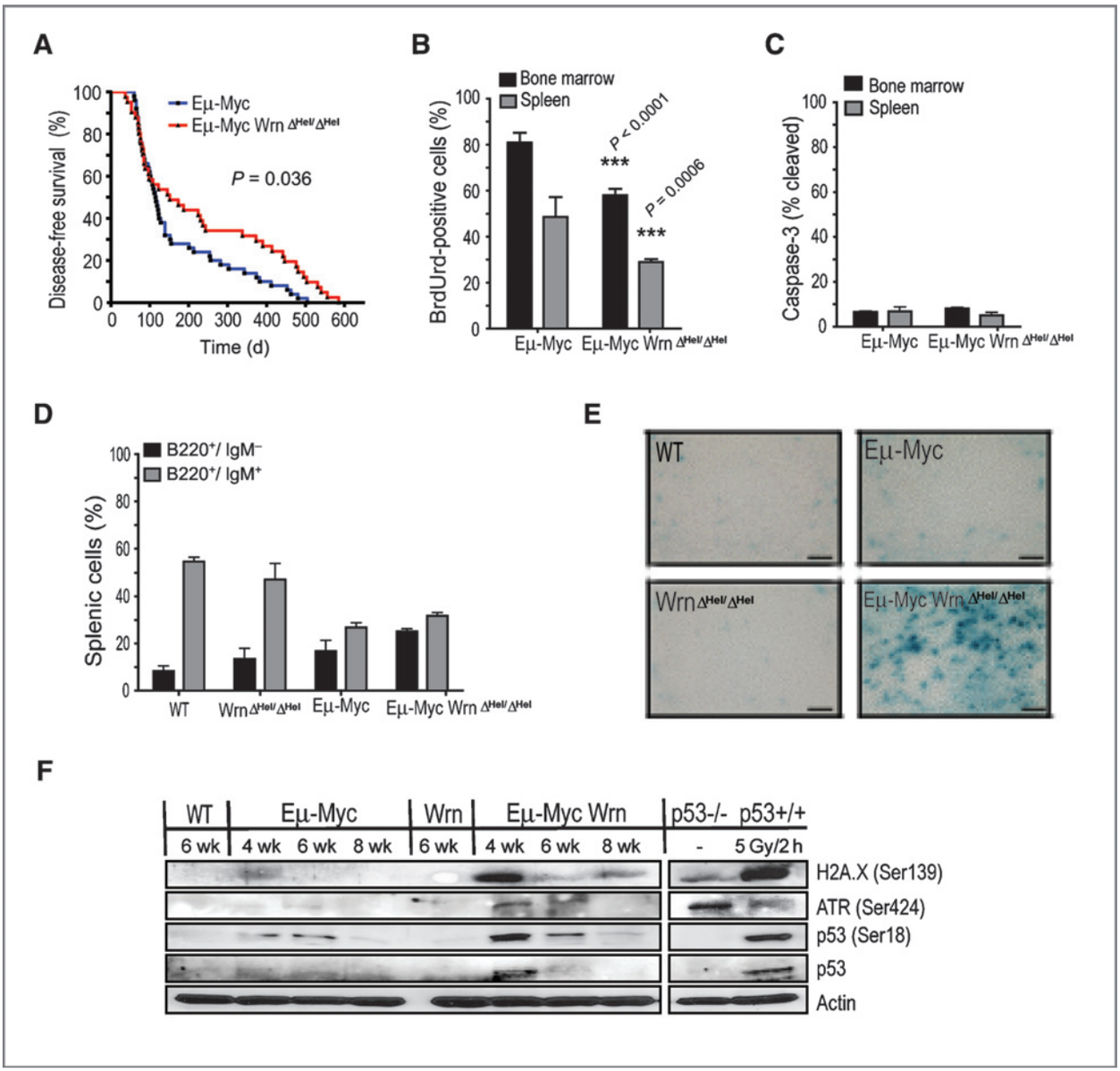

Figure 3. Werner deficiency (Wrn $^{\Delta hel/\Delta hel}$) delays lymphomagenesis. A, Kaplan–Meier curves showing disease-free survival of Eμ-Myc (median survival of 115 days) and Eμ-Myc Wrn $^{\Delta hel/\Delta hel}$ (median survival of 151 days) mice; significant difference via logrank test, $P = 0.036$. B, flow-cytometry analysis of BrdUrd-positive cells as a measure of proliferation; unpaired *t* tests, bone marrow: ***, $P < 0.0001$, spleen: ***, $P = 0.0006$. C, flow-cytometry analysis of cleaved caspase-3 as a measure of apoptosis. D, splenic pre-B cells ($B220^+/IgM^-$) and mature B cells ($B220^+/IgM^+$) from Eμ-Myc and Eμ-Myc $Wrn^{\Delta hel/\Delta hel}$ mice; matched littermates ($n = 2$) from 4-week mice of all genotypes were analyzed in triplicate in panels B, C, and D. E, acidic B-galactosidase staining of germinal center lymphoid follicles from spleens of 4- to 6-week-old mice of the indicated genotype. Images are representative of 3 mice of each genotype. Scale bar represents 40 μm. F, longitudinal analysis of protein levels from splenocytes isolated from mice at 4, 6, and 8 weeks. Antibodies to phospho-histone H2A.X (Serine 139), phospho-Atr (Serine 428), phospho-p53 (Serine 18), and p53 were used, and actin is shown as a loading control. WT refers to wild-type control, Wrn refers to $Wrn^{\Delta hel/\Delta hel}$, $p53^{-/-}$ and $p53^{+/+}$ to splenocytes isolated from 6-week-old mice, $p53^{+/+}$ ($p19^{-/-}$) mice were irradiated with 5Gy (^{137}Cs) and splenocytes isolated 2 hours later.

that in the context of a *p53* mutant background, Wrn deficiency leads to a significant increase in DNA damage (γ-H2AX) and reduces proliferation (phospho-H3) and apoptosis (TUNEL; Supplementary Fig. S4A and S4B). Upon closer examination of *p53* mutant tumors, nuclear accumulation of p53 seems more pronounced in *Eμ-Myc* $Wrn^{\Delta hel/\Delta hel}$ lymphomas with a concordant increase in senescence-associated β-galactosidase (Fig. 4B). These results confirmed that a defect in Wrn activity leads to engagement of antiproliferative/senescence pathways, likely through the combined effects of the tumor suppressors $p16^{Ink4a}/p19^{Arf}$ and this does not require wild-type p53.

Published OnlineFirst February 1, 2012; DOI:10.1158/1541-7786.MCR-11-0508

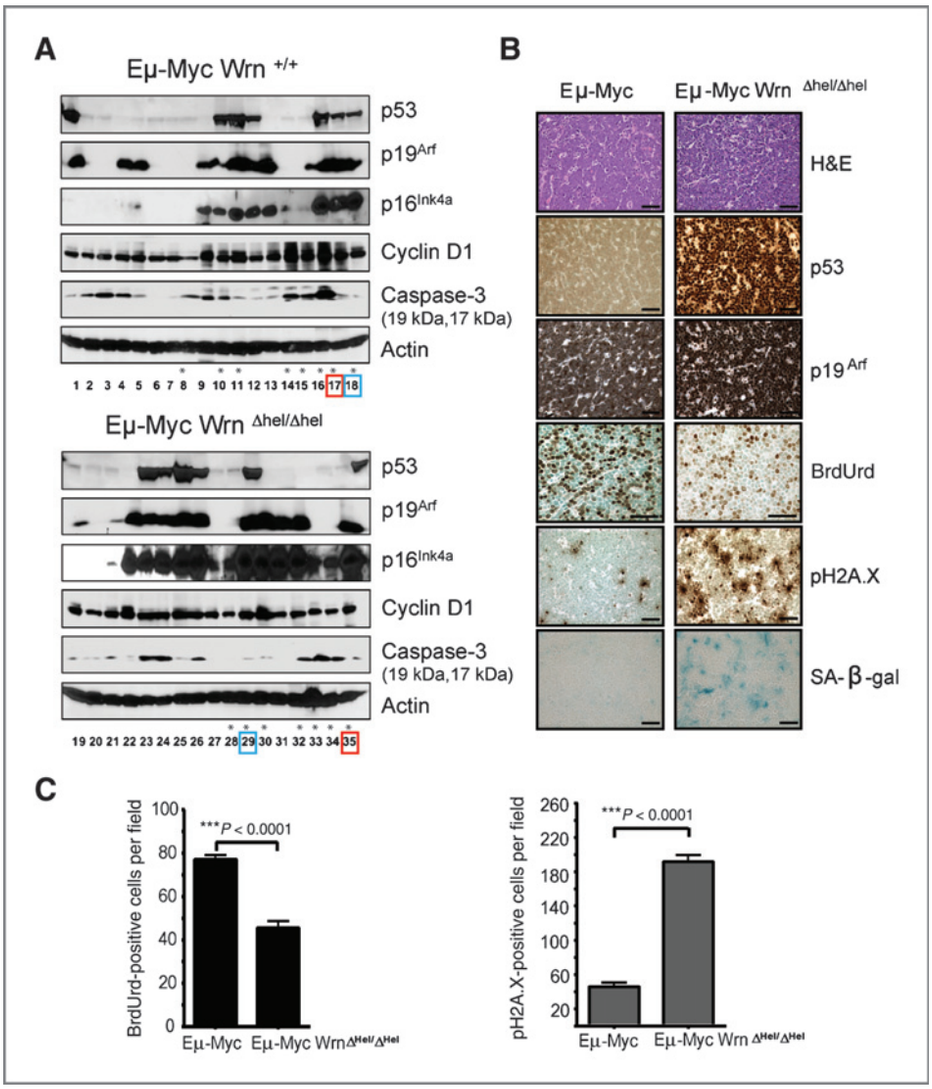

Figure 4. Molecular profiling of Eμ-Myc and Eμ-Myc Wrn$^{\Delta hel/\Delta hel}$ lymphomas. A, representative immunoblot of Eμ-Myc (lanes 1–18) and Eμ-Myc Wrn $^{\Delta hel/\Delta hel}$ (lanes 19–35) lymphomas showing levels of p53, p19^{Arf}, p16^{Ink4a}, cyclin D1, cleaved caspase-3, and actin (loading control). Late onset lymphomas are denoted with an asterisk and represent 8 lymphomas arising in Eμ-Myc mice (range: 121–505 days), and 7 lymphomas arising in Eμ-Myc Wrn$^{\Delta hel/\Delta hel}$ (range: 122–495 days). Red and blue boxes refer to the mice used for IHC analysis in Supplementary Fig. S4A. B, representative photomicrographs of Eμ-Myc and Eμ-Myc Wrn$^{\Delta hel/\Delta hel}$ lymphomas with p53 overexpressed (i.e., *p53* mutation, ref. 16) and p19^{Arf} overexpression, immunohistochemically stained for p53, p19^{Arf}, BrdUrd, H2A.X (serine 139), and senescence-associated β-galactosidase (SA-β-gal); scale bar on all images represents 100 μm. C, immunohistochemical scoring of Eμ-Myc and Eμ-Myc Wrn$^{\Delta hel/\Delta hel}$ lymphomas for proliferation (BrdUrd) and DNA damage (H2A.X Serine 139) of photomicrographs in B. Columns represent mean ± SEM ($n = 10$, 40× and 100× fields, respectively; unpaired *t* tests, BrdUrd: ***, $P < 0.0001$, *H2A.X*: ***, $P < 0.0001$).

Global gene expression analysis of Wrn-deficient lymphomas identifies TAp63 as a possible mediator of senescence response

To globally define the pathways by which Wrn deficiency impairs tumor development, microarray gene expression analysis was done on 4 lymphomas from each *Wrn* genotype (Supplementary Table S1, GSE25671). Ingenuity Pathway Analysis, based on known literature connections, of significantly upregulated genes in Wrn-deficient versus Wrn wild-type lymphomas identified genes that centered on the p53 homolog TAp63, the *Cdkn2*a (p16^{Ink4a}/p19^{Arf}) locus, and the p53-dependent stress-inducible nuclear protein, Trp53inp1 (Fig. 5A, Supplementary Table S1A). TAp63 has recently been recognized as an key mediator of senescence (21). Quantitative RT-PCR confirmed increased expression of TAp63 in additional *Eμ-Myc Wrn*$^{\Delta hel/\Delta hel}$ lymphomas (Supplementary Fig. S3). Furthermore, induction of TAp63 was recapitulated *in vitro* by acute knockdown of Wrn in *Eμ-Myc* lymphoma-derived cells with *p53* mutation (Fig. 5B and Supplementary Fig. S5). In addition, CDK inhibitors such as Cdkn1c (p57Kip2), and Cdkn1b (p27Kip1), were among the upregulated genes in *Eμ-Myc Wrn*$^{\Delta hel/\Delta hel}$ lymphomas (GSE25671). All together, the results obtained by global gene expression analysis correlated with the data derived from the immunohistochemical and biochemical assessment of lymphoma tissue and delineate a senescence signature associated with *Eμ-Myc Wrn*$^{\Delta hel/\Delta hel}$ lymphomas. In addition, they suggested that TAp63 could be the primary mediator of a senescence response in *p53* mutant tumors.

Discussion

The RecQ DNA helicase WRN, has previously been associated with tumor suppression, as Werner Syndrome patients, in addition to premature aging, develop rare mesenchymal tumors late in life (5). In contrast, we hypothesized that WRN, by preventing senescence of cancer cells, could contribute to the tumorigenic process.

Published OnlineFirst February 1, 2012; DOI:10.1158/1541-7786.MCR-11-0508

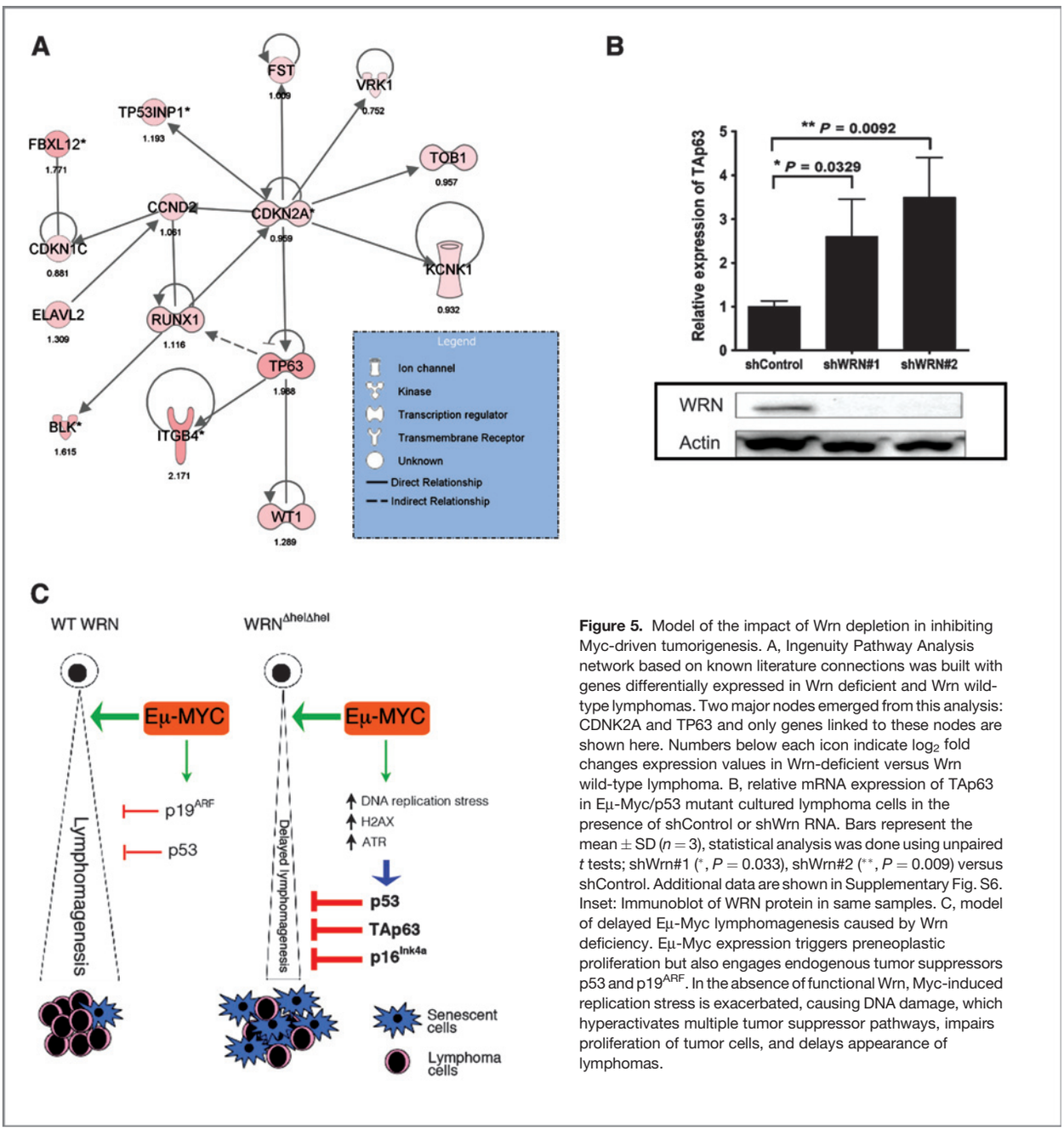

Figure 5. Model of the impact of Wrn depletion in inhibiting Myc-driven tumorigenesis. A, Ingenuity Pathway Analysis network based on known literature connections was built with genes differentially expressed in Wrn deficient and Wrn wild-type lymphomas. Two major nodes emerged from this analysis: CDNK2A and TP63 and only genes linked to these nodes are shown here. Numbers below each icon indicate $\log_2$ fold changes expression values in Wrn-deficient versus Wrn wild-type lymphoma. B, relative mRNA expression of TAp63 in Eμ-Myc/p53 mutant cultured lymphoma cells in the presence of shControl or shWrn RNA. Bars represent the mean ± SD ($n = 3$), statistical analysis was done using unpaired *t* tests; shWrn#1 (*, $P = 0.033$), shWrn#2 (**, $P = 0.009$) versus shControl. Additional data are shown in Supplementary Fig. S6. Inset: Immunoblot of WRN protein in same samples. C, model of delayed Eμ-Myc lymphomagenesis caused by Wrn deficiency. Eμ-Myc expression triggers preneoplastic proliferation but also engages endogenous tumor suppressors p53 and $p19^{ARF}$. In the absence of functional Wrn, Myc-induced replication stress is exacerbated, causing DNA damage, which hyperactivates multiple tumor suppressor pathways, impairs proliferation of tumor cells, and delays appearance of lymphomas.

This hypothesis was supported by our previous studies showing that the MYC oncoprotein directly stimulates transcription of the *WRN* gene, and in turn, loss of WRN function leads to senescence of MYC overexpressing cells (1). This codependence of WRN and MYC overexpression was attributed to the role of WRN in limiting replication-associated damage during S-phase, a process that is dramatically accelerated in MYC overexpressing cells through direct association of MYC with the prereplication machinery (2, 3).

To determine whether MYC-driven cancers depend on Wrn in an *in vivo* setting, we investigated 2 models of Myc-associated tumorigenesis, as well as the effect of both acute and chronic Wrn depletion on tumor growth. The acute depletion of WRN was carried out with NSCLC A549 cells which express high levels of c-MYC and have been optimized for the conditional knockdown of WRN *in vivo*. In addition, the use of a Myc-driven mouse model allowed us to test the consequences of chronically interfering with a helicase-defective Wrn protein, much like one would envision in a therapeutic setting with small molecule inhibitors to the Wrn helicase domain. Both models showed consistent results, that is, impairment of WRN function profoundly effects tumor growth due to excessive accumulation of DNA

Published OnlineFirst February 1, 2012; DOI:10.1158/1541-7786.MCR-11-0508

damage and decreased proliferation with consequent senescence (observed in the Eμ-Myc lymphoma) or prominent necrosis (as observed in the A459 xenograft model). Wrn helicase deficiency effectively delayed the insurgence of lymphomas through activation of 2 tumor suppressors: $p16^{Ink4a}$ and TAp63 (see model in Fig. 5C). Importantly, we were able to recapitulate in lymphoma cells from *Eμ-Myc* mice that acute depletion of Wrn also induces TAp63, even in a p53 mutant setting (Fig. 5 and Supplementary Fig. S5). Our results are consistent with a recent report of increased senescence and delayed lymphomagenesis in *Eμ-Myc* $p53^{515C/+}$ and *Eμ-Myc* $p53^{515C/515C}$ mutant mice relative to *Eμ-Myc* $p53^{+/-}$ mice (30) and highlight a mechanism of growth arrest and cellular senescence that has relevance for future therapeutic application of WRN inhibitors even in the context of p53 mutant cancers. In this view, the endogenous DNA damage generated by Wrn deficiency acts not unlike the damage generated via genotoxic treatment or telomere shorting to engage tumor suppressor pathways (31, 32). The effect of Wrn depletion was lost in p53-deficient backgrounds (3), and Wrn deficiency increased the rate of cancer in a p53-deficient background (33), suggesting that complete loss of function of p53 could disable the senescence response in Wrn-deficient cancer cells. Additional model systems will be needed to distinguish the impact of p53 deletion versus mutation on Wrn function.

It is worthwhile to note that the Kaplan–Meier curves comparing *Eμ-Myc Wrn* wild type with $Wrn^{\Delta hel/\Delta hel}$ indicated an age-dependent penetrance of tumor suppression caused by Wrn deficiency. Although this requires further investigation, one hypothesis that is consistent with the observed elevation of $p16^{Ink4a}$ in Wrn-deficient tumors is that Wrn deficiency, superimposed with the natural aging of hematopoietic precursors (also characterized by an elevation of $p16^{Ink4a}$), may additively provide a barrier for late onset tumor development (34). A second hypothesis is derived from the report that late onset lymphomas in *Eμ-Myc* mice are distinct from early onset tumors with respect to differentiation status and signaling pathways, such as those regulated by NF-κB (35). Differential activation of these pathways may modify the impact of Wrn deficiency on engaging antiproliferative pathways.

Our studies also highlight the differential sensitivity of cancer cells versus normal cells to loss of WRN. This is reminiscent of other reports of tumor-specific sensitivity to loss of DNA repair function. For example, mice deficient in NHEJ activity due to mutation in *Prkdc* (the catalytic subunit of DNA-dependent protein kinase) are normal, barring a defect in V(D)J recombination. However, they are markedly resistant to development of squamous cell carcinoma, indicating active NHEJ is necessary for optimal tumor growth (36). Furthermore, a recent study indicates that Atr deficiency also protects mice from Myc-driven lymphomas (37). In contrast, Atm deficiency by eliminating a DNA damage–induced apoptotic response accelerates Myc-driven tumorigenesis (38), highlighting differences in DNA damage pathways and their relation to Myc. This principle of differential sensitivity of cancer versus normal cells to DNA repair deficiency has important therapeutic potential, as in the case of use of PARP inhibitors for cancers deficient in BRCA1 or BRCA2 function (39). Similarly, therapeutics directed against RecQ helicases may prove beneficial for cancers with amplification/alterations of MYC by marshaling the DNA damage response and intrinsic tumor suppressor pathways. Our experiments directly addressed the effects of a WRN helicase mutant in tumor growth, thus pinpointing not just the gene, but also the domain that could be targeted by small molecules. The catalytic activity of this domain necessitates both ATP binding and ATPase activity (4) and, as such, is highly druggable (40). Thus, targeting WRN or its enzymatic functions could prove to be an effective strategy to treat MYC-associated cancers.

Disclosure of Potential Conflicts of Interest

No potential conflicts of interest were disclosed.

Authors' Contributions

Conception and design: R. Moser, M. Toyoshima, C.J. Kemp, C. Grandori
Development of methodology: R. Moser, M. Toyoshima, K.E. Gurley, C.J. Kemp
Acquisition of data (provided animals, acquired and managed patients, provided facilities, etc.): R. Moser, M. Toyoshima, K. Robinson, K.E. Gurley
Analysis and interpretation of data (e.g., statistical analysis, biostatistics, computational analysis): R. Moser, M. Toyoshima, J. Davison, M. Morgan, C.J. Kemp, C. Grandori
Writing, review, and/or revision of the manuscript: R. Moser, M. Toyoshima, K. Robinson, H.L. Howie, J. Davison, C.J. Kemp, C. Grandori
Administrative, technical, or material support (i.e., reporting or organizing data, constructing databases): R. Moser, M. Toyoshima, K. Robinson
Study supervision: C.J. Kemp, C. Grandori

Acknowledgments

The authors thank Dr. Ray Monnat and Dr. Julia Sidorova for critically reviewing the manuscript, Dr. Denise Galloway and her laboratory for support and guidance during the course of this work, Dr. Patrick Paddison and Dr. Dusty Miller for viral vectors utilized for *Wrn* knockdown experiments, and Dr. C.A. Schmitt for retroviral infection protocols and advice.

Grant Support

This work was supported by R01 grants NIA AG02661, NCI CA099517, and the NCI Mouse Models of Human Cancer Consortium. J. Davison and M. Morgan were supported in part by NIH P30 CA015704.

The costs of publication of this article were defrayed in part by the payment of page charges. This article must therefore be hereby marked *advertisement* in accordance with 18 U.S.C. Section 1734 solely to indicate this fact.

Received October 20, 2011; revised January 25, 2012; accepted January 26, 2012; published OnlineFirst February 1, 2012.

References

1. Grandori C, Wu KJ, Fernandez P, Ngouenet C, Grim J, Clurman BE, et al. Werner syndrome protein limits MYC-induced cellular senescence. Genes Dev 2003;17:1569–74.

2. Dominguez-Sola D, Ying CY, Grandori C, Ruggiero L, Chen B, Li M, et al. Non-transcriptional control of DNA replication by c-Myc. Nature 2007;448:445–51.

Published OnlineFirst February 1, 2012; DOI:10.1158/1541-7786.MCR-11-0508

3. Robinson K, Asawachaicharn N, Galloway DA, Grandori C. c-Myc accelerates S-Phase and requires WRN to avoid replication stress. PLoS One 2009;4:e5951.
4. Chu WK, Hickson ID. RecQ helicases: multifunctional genome caretakers. Nat Rev Cancer 2009;9:644–54.
5. Rossi ML, Ghosh AK, Bohr VA. Roles of Werner syndrome protein in protection of genome integrity. DNA Repair (Amst) 2010;9:331–44.
6. Gray MD, Shen JC, Kamath-Loeb AS, Blank A, Sopher BL, Martin GM, et al. The Werner syndrome protein is a DNA helicase. Nat Genet 1997;17:100–3.
7. Shen JC, Gray MD, Oshima J, Kamath-Loeb AS, Fry M, Loeb LA. Werner syndrome protein. I. DNA helicase and DNA exonuclease reside on the same polypeptide. J Biol Chem 1998;273:34139–44.
8. Brosh RM Jr, Waheed J, Sommers JA. Biochemical characterization of the DNA substrate specificity of Werner syndrome helicase. J Biol Chem 2002;277:23236–45.
9. Compton SA, Tolun G, Kamath-Loeb AS, Loeb LA, Griffith JD. The Werner syndrome protein binds replication fork and Holliday junction DNAs as an oligomer. J Biol Chem 2008;283:24478–83.
10. Aggarwal M, Sommers JA, Morris C, Brosh RM Jr. Delineation of WRN helicase function with EXO1 in the replicational stress response. DNA Repair (Amst) 2010;9:765–76.
11. Sidorova JM, Li N, Folch A, Monnat RJ Jr. The RecQ helicase WRN is required for normal replication fork progression after DNA damage or replication fork arrest. Cell Cycle 2008;7:796–807.
12. Krasnoselsky AL, Whiteford CC, Wei JS, Bilke S, Westermann F, Chen QR, et al. Altered expression of cell cycle genes distinguishes aggressive neuroblastoma. Oncogene 2005;24:1533–41.
13. Lombard DB, Beard C, Johnson B, Marciniak RA, Dausman J, Bronson R, et al. Mutations in the WRN gene in mice accelerate mortality in a p53-null background. Mol Cell Biol 2000;20:3286–91.
14. Lebel M, Leder P. A deletion within the murine Werner syndrome helicase induces sensitivity to inhibitors of topoisomerase and loss of cellular proliferative capacity. Proc Natl Acad Sci U S A 1998;95:13097–102.
15. Adams JM, Harris AW, Pinkert CA, Corcoran LM, Alexander WS, Cory S, et al. The c-myc oncogene driven by immunoglobulin enhancers induces lymphoid malignancy in transgenic mice. Nature 1985;318:533–8.
16. Eischen CM, Weber JD, Roussel MF, Sherr CJ, Cleveland JL. Disruption of the ARF-Mdm2-p53 tumor suppressor pathway in Myc-induced lymphomagenesis. Genes Dev 1999;13:2658–69.
17. Bandyopadhyay D, Gatza C, Donehower LA, Medrano EE. Analysis of cellular senescence in culture *in vivo*: the senescence-associated beta-galactosidase assay. Curr Protoc Cell Biol 2005 Chapter 18: Unit 18 19.
18. Dimri GP, Lee X, Basile G, Acosta M, Scott G, Roskelley C, et al. A biomarker that identifies senescent human cells in culture and in aging skin *in vivo*. Proc Natl Acad Sci U S A 1995;92:9363–7.
19. Kruisbeek AM. *In vitro* assays for mouse B and T cell function. Curr Protoc Immunology 2000 Supplement 39: Unit 3.1.3.
20. Wang YV, Leblanc M, Wade M, Jochemsen AG, Wahl GM. Increased radioresistance and accelerated B cell lymphomas in mice with Mdmx mutations that prevent modifications by DNA-damage-activated kinases. Cancer Cell 2009;16:33–43.
21. Guo X, Keyes WM, Papazoglu C, Zuber J, Li W, Lowe SW, et al. TAp63 induces senescence and suppresses tumorigenesis in vivo. Nat Cell Biol 2009;11:1451–7.
22. Keyes WM, Wu Y, Vogel H, Guo X, Lowe SW, Mills AA. p63 deficiency activates a program of cellular senescence and leads to accelerated aging. Genes Dev 2005;19:1986–99.
23. Smyth GK. Limma: linear models for microarray data. In: 'Bioinformatics and Computational Biology Solutions using R and Bioconductor', 1 edition, p. 397-420. New York: Springer, 2005.
24. Benjamini Y, Hochberg Y. Controlling the false discovery rate: a practical and powerful approach to multiple testing. J Royal Stat Soc B 1995:289–300.
25. Edgar R, Domrachev M, Lash AE. Gene expression omnibus: NCBI gene expression and hybridization array data repository. Nucleic Acids Res 2002;30:207–10.
26. Eischen CM, Woo D, Roussel MF, Cleveland JL. Apoptosis triggered by Myc-induced suppression of Bcl-X(L) or Bcl-2 is bypassed during lymphomagenesis. Mol Cell Biol 2001;21:5063–70.
27. Sharpless NE, Bardeesy N, Lee KH, Carrasco D, Castrillon DH, Aguirre AJ, et al. Loss of p16Ink4a with retention of p19Arf predisposes mice to tumorigenesis. Nature 2001;413:86–91.
28. Sherr CJ, Roberts JM. CDK inhibitors: positive and negative regulators of G1-phase progression. Genes Dev 1999;13:1501–12.
29. Sherr CJ, Bertwistle D, DEN Bertwistle W, Kuo ML, Sugimoto M, Tago K, et al. p53-Dependent and -independent functions of the Arf tumor suppressor. Cold Spring Harb Symp Quant Biol 2005;70:129–37.
30. Post SM, Quintas-Cardama A, Terzian T, Smith C, Eischen CM, Lozano G. p53-dependent senescence delays Emu-myc-induced B-cell lymphomagenesis. Oncogene 2010;29:1260–9.
31. Feldser DM, Greider CW. Short telomeres limit tumor progression *in vivo* by inducing senescence. Cancer Cell 2007;11:461–9.
32. Schmitt CA, Fridman JS, Yang M, Lee S, Baranov E, Hoffman RM, et al. A senescence program controlled by p53 and p16INK4a contributes to the outcome of cancer therapy. Cell 2002;109:335–46.
33. Lebel M, Cardiff RD, Leder P. Tumorigenic effect of nonfunctional p53 or p21 in mice mutant in the Werner syndrome helicase. Cancer Res 2001;61:1816–9.
34. Signer RA, Montecino-Rodriguez E, Witte ON, Dorshkind K. Aging and cancer resistance in lymphoid progenitors are linked processes conferred by p16Ink4a and Arf. Genes Dev 2008;22:3115–20.
35. Mori S, Rempel RE, Chang JT, Yao G, Lagoo AS, Potti A, et al. Utilization of pathway signatures to reveal distinct types of B lymphoma in the Emicro-myc model and human diffuse large B-cell lymphoma. Cancer Res 2008;68:8525–34.
36. Kemp CJ, Vo K, Gurley KE. Resistance to skin tumorigenesis in DNAPK-deficient SCID mice is not due to immunodeficiency but results from hypersensitivity to TPA-induced apoptosis. Carcinogenesis 1999;20:2051–6.
37. Murga M, Campaner S, Lopez-Contreras AJ, Toledo LI, Soria R, Montana MF, et al. Exploiting oncogene-induced replicative stress for the selective killing of Myc-driven tumors. Nat Struct Mol Biol 2011;18:1331–5.
38. Maclean KH, Kastan MB, Cleveland JL. Atm deficiency affects both apoptosis and proliferation to augment Myc-induced lymphomagenesis. Mol Cancer Res 2007;5:705–11.
39. Fong PC, Boss DS, Yap TA, Tutt A, Wu P, Mergui-Roelvink M, et al. Inhibition of poly(ADP-ribose) polymerase in tumors from BRCA mutation carriers. N Engl J Med 2009;361:123–34.
40. Aggarwal M, Sommers JA, Shoemaker RH, Brosh RM Jr. Inhibition of helicase activity by a small molecule impairs Werner syndrome helicase (WRN) function in the cellular response to DNA damage or replication stress. Proc Natl Acad Sci U S A 2011;108:1525–30.